

RCS MEASUREMENTS- FOCUS ON NEAR-FIELD RCS MEASUREMENTS

Anjali Bhatia, Defence Laboratory, DRDO, Jodhpur

This talk overviews RCS Measurements with emphasis on measuring large, full-scale targets. High-resolution images, and far-field patterns are the normally required outputs of an RCS study. The focus is on Near-Field RCS Measurements, i.e. how to get the same information out by measurements made at short ranges.

Scattering is closely analogous to radiation from Antennas. The difference is that Antennas are designed for a particular radiation pattern, by using a feed to create a current distribution over a metallic surface. In scattering, the currents result from illumination by external incident fields. Because the currents have not been designed for a particular directivity, in general, all direction scattering of the fields is observed.

The scattered fields are determined in the same manner as radiation from an arbitrary antenna current distribution - if the induced currents are known. The big problem is to calculate or estimate these currents, induced in response to the incident EM field. The induced currents can be determined by enforcing the boundary conditions at the material interface. As with antennas, the currents can be computed using Method of Moments and other techniques. However exact determination of these currents is a problem of significant complexity. Simplifying assumptions on the current distributions can be used in some cases.

We would like to be able to measure the scattered field distribution to validate computations, or when the target is too complex to handle computationally (which is very often the case). The Term Radar Cross-Section is used to quantify this scattering. Bi-static RCS is the generalized behavior- where the 3D scattering pattern is quantified for every desired illumination angle. In a simplified requirement, Monostatic RCS quantifies the scattering where only the backscatter back along the incident direction is of interest.

To quantify this scattering, the term Radar Cross-Section is used. This term, σ , describes the ratio of the power scattered per unit solid angle in the direction of interest, to the incident power density in W / m^2 from the direction of illumination.

$$\begin{aligned}W_i &= \frac{P_t G_t}{4\pi R^2} \text{ Watts/ sq m} \\P_{\text{intercepted}} &= W_i \sigma_G \text{ Watts} \\P_{\text{scattered}} &= \rho_s P_{\text{intercepted}} = \rho_s W_i \sigma_G \text{ Watts} \\P_{\text{scattered}_\theta} &= D_\theta P_{\text{scattered}} = D_\theta \rho_s W_i \sigma_G \text{ sq m} \\P_{\text{received}} &= \frac{P_{\text{scattered}_\theta} A_e}{4\pi R^2} = \left(\frac{P_t G_t}{4\pi R^2} \right) (D_\theta \rho_s \sigma_G) \left(\frac{A_e}{4\pi R^2} \right) \text{ Watts} \\&= \left(\frac{P_t G_t}{4\pi R^2} \right) (\sigma_\theta) \left(\frac{A_e}{4\pi R^2} \right) \text{ Watts}\end{aligned} \tag{Eq 1}$$

The RCS is seen to factor in 3 effects- that of the geometric cross-section which intercepts the incident energy, the object reflectivity, which describes the portion of the intercepted energy that is scattered, and the directivity, which describes how the scattered energy is angularly distributed.

By definition, the illumination is planar- and thus the relative phase of the incident wavefront over the object is definitive and range independent.

The measurement of RCS thus is analogous to Antenna Pattern Measurements. Just as the output is a 3D gain pattern for antennas, the RCS quantifies a 3D scattering pattern- however one such scattering pattern is defined for each angle of incidence. Just as with antennas, the RCS must be measured at far-field distances.

The differences are

1. The stimulus must be provided in the form of an external illuminating plane wavefront from the desired direction- unlike feed currents for antennas
2. Antennas are designed to have well behaved and directive gain patterns- whereas RCS patterns have an ill-defined complex presentation- unless specifically designed to be otherwise.
3. Antenna radiators are typically planar, or with the depth element relatively small compared to span- while target depths can be anything.
4. Measurements for antennas are required over the small antenna design band, while typically wideband information is required for RCS

So, to measure the bi-static RCS_{θ_i, θ_j} we need to generate a clean planar illumination from the incident direction θ_i , and measure the power reflected back in the directions θ_j , with the receiver at far-field distance (where the propagating fields have only an angular dependence). The scattering behaviour of an object would be completely characterized by the complete 4π steradian scattering pattern (i) for each incident angle in 3D space, (ii) at all frequencies, and (iii) for co and cross polarizations for both polarizations.

Such an RCS measurement carries all the requirements associated with Antenna Measurements, and more. The Far-Field Distance must be maintained between target and Antennas used for Transmit and Receive. The Measurement Zone must be clutter free. A clean Plane Wave must illuminate the target – without multipath contributions. The reflected energy returning to the receive antenna must not be contaminated by surrounding clutter and multipath effects. Precise positioning systems must be available to accurately configure the Look Angles for the RCS measurement. The Target Support Structure must not contribute to the RCS, and must not couple to the Target.

Although the Do and Don't constraints are simple and straightforward, implementing them in practice takes up the major portion in cost and complexity of a measurement, and contributes the major uncertainty in the measured results.

Far-Field Criteria

The far-field criterion is essential for defining RCS because only under this assumption does the signature become range independent. The illumination of the test object by a plane wave ensures that the reflections from the individual parts of the object are added after being weighted by well-defined relative path phase factors. If the illumination is phase is spherical, the path phase factors will depend on the radius of the sphere, which in turn depends on the distance from source to target.

In computations it is easy to adhere to the far-field criteria. However, with actual measurements, the finite distance from a point source to target means that the plane wave illumination can only be approximately achieved. (Except in Compact Ranges which are especially designed to provide planar illumination.) By the standard far-field

criterion of $2D^2 / \lambda$, it is ensured that the phase deviation from plane wave illumination is limited to a maximum of $\lambda/8$, or 45 deg, over the span of the test object. While this may be adequate for antenna measurements which have a well defined mainlobe, it may not be adequate for RCS patterns which are more irregular and broad. The deviation from the assumed to the actual phase of illumination gives rise to pattern uncertainties, including null-filling, and increase in sidelobes. However, even to meet the standard far-field criteria, the far-field distance requirement for measuring large objects quickly becomes impractically large and unmanageable.

The alternate solution to huge RCS ranges is the Compact range – where reflectors collimate the incident fields to achieve planar illumination. Very large compact ranges are needed to accommodate targets of sizes of the order of 10-20 m, so a huge cost and complexity factor is involved here also.

RCS Measurements

At high frequencies scattering from a complex target is a vector resultant of scattering contributions from discrete scattering centers weighted by their path length phase factors. Because of this, the RCS of complex objects are complex patterns with frequency and look-angle, and a single (spot) frequency, spot angle measurement of the composite target rarely carries any import- as this is only one possible weighted combination of the individual scattering centers on the object. We require data over a wide range of angles and frequencies to derive meaningful statistics for the target.

The RCS details must be captured over an angular space and frequency sector, with minimum sampling requirements. Undersampling captures the general envelope of the RCS pattern sufficiently well. However, sampling requirements must be met if the data matrix is to be transformed to a Scattering Map (Image).

The sampling requirements are dictated by the size of the object: $\Delta\theta \leq \lambda/2D$, $\Delta f \leq c/2D$. If an object has significant multiple scattering interactions contributing to its signature, even finer sampling in angle is required because the multiple scattering gives rise to changes in measurement phase in excess of those expected due to rotation of the body alone. The apparent extent of the object now exceeds its physical dimensions.

RCS Imaging

Measuring the composite RCS of the complex body gives only a weighted summation of the individual contributors; it gives nil information on the individual contributions themselves.

$$R = \sum_i r_i \exp\left(\frac{-j2\pi f d_i}{c}\right) \quad \text{Eq 2}$$

It is useful to resolve the net RCS to these individual contributions. Imaging techniques allow us to do this. Imaging provides a spatial mapping of the origins of backscattered radiation from an illuminated object

Under the conditions when the composite scattering can be modeled to be a vector summation of Individual Contributions, a very simple Fourier Transform Relationship exists between the Spatial Domain (Reflectivity distribution in 3D space) and the Bi-static Measurement Domain against frequency, incident angle, and reflected angle (also called p-space)[1]

$$\Gamma(\hat{\theta}_i, \hat{\theta}_r, k) = \Gamma(\bar{p}) = \int_{S_{\text{illuminated}}} O(\bar{r}') e^{j\bar{p} \cdot \bar{r}'} dS' \quad \text{Eq 3}$$

$$\bar{p} = \bar{k}_i - \bar{k}_r = k(\hat{\theta}_i - \hat{\theta}_r) = 2k \cos \frac{\beta}{2} \hat{\theta}_p$$

There are three variables k, θ_r, θ_i which we can use to access the Fourier Space Data $\Gamma(\bar{p})$. One is directly related to frequency, and the other two relate to the aspects along which the object is illuminated, and measured. The Ewald Sphere representation shows the Fourier Space sample location in (p_x, p_y) space. For a given incident direction, the corresponding Ewald sphere is centered at k_i and has radius k (Figure 1).

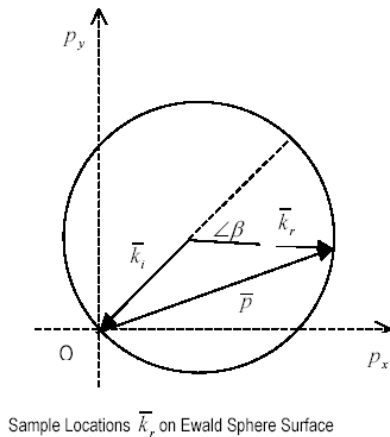


Figure 1 Sampling Locations on surface of Ewald Sphere

The implication is that any far-field reflectivity measurement made on the object, at a given frequency, a given incidence angle, and a given observation angle, gives us a data point in Fourier Space corresponding to $\Gamma(k, \theta_r, \theta_i)$. Data points can be sampled in Fourier Space by varying any or all of k, θ_r, θ_i . Changing the direction of incidence shifts the center of the Ewald Sphere. Changing the frequency changes the radius of the sphere. Changing the direction of the receiving antenna moves the bi-static sampled location over the sphere surface. For a given bistatic angle β , the sampled Fourier Space Data are distributed along a radial line along $\hat{\theta}_p$.

When monostatic data is acquired, $\hat{\theta}_r = -\hat{\theta}_i = -\hat{\theta}$ and $\bar{p} = k(\hat{\theta}_r - \hat{\theta}_i) = 2k\hat{\theta}$. Sampling over the Ewald Sphere now takes place along the surface of spheres centered at the origin (Figure 2), with radius equal to twice k . The frequency is varied to change the radius of the sphere, and the look angle variation provides data over the sphere's surface, providing data points over an annular ring. The bistatic data point corresponding to frequency k_0 and bistatic angle θ are mapped to the point $(2k_0 \cos(\theta/2), k_0 \sin \theta)$. A bistatic measurement at angle θ therefore corresponds to a monostatic measurement at angle $\theta/2$, at a frequency that has been shifted to $k_0 \cos(\theta/2)$.

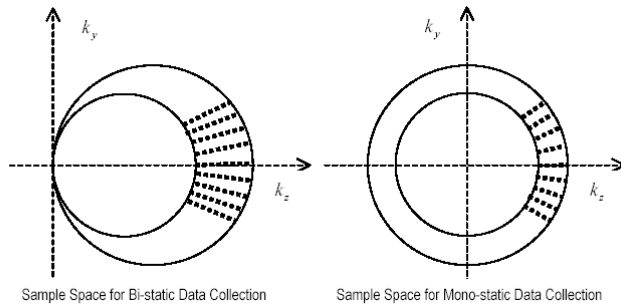


Figure 2 Sample Space in (i) Bi-static and (ii) Mono-static Data Collection

Once we have samples in the Fourier Space, extracting the 3D object reflectivity function is theoretically obtainable by Fourier Transform of the p-space data. However, the samples obtained by conventional measurements (monostatic/ bistatic) are not available over a regular 3D Cartesian grid. Hence interpolation becomes necessary if conventional Cartesian Transform algorithms are to be used. For the special case of 2D monostatic RCS data, the samples are obtained over a polar grid $(2k, \theta)$. Hence the Fourier Transform as expressed in polar coordinates can also be used for constructing the image.

The spectral domain (p-space) data are available over $(2k, \theta, \phi)$. However the Cartesian counterparts of (x, y, z) are (k_x, k_y, k_z) in Fourier Space. They are related as

$$k_x = 2k \cos \theta \cos \phi, \quad k_y = 2k \cos \theta \sin \phi, \quad k_z = 2k \sin \theta$$

To collect this Fourier Space data requires (i) Multi-frequency data- which gives the down range resolution, and (ii) Multi-aspect data- which gives resolution in the cross-range.

Effect of Finite Data Set

The object reflectivity function $O(\vec{r}')$ in (x, y, z) space is naturally confined to the extent of the object boundaries. Because of this, the spectral extent of the p-space data is not contained within an upper limit. To reconstruct $O(\vec{r}')$ with complete fidelity will require that the p-space be fully sampled. In a practical situation, measurements are taken over a finite band of frequencies $B = [f_1, f_2]$, and over a finite set of look angles $[\theta_1, \theta_2]$. The effect of truncating the full spectral content is equivalent to multiplying the p-space data by a window function. The effect in the spatial domain is that the reflectivity function is convolved with the window's response, resulting in a low-frequency filtering of the spatial data, with corresponding loss of resolution.

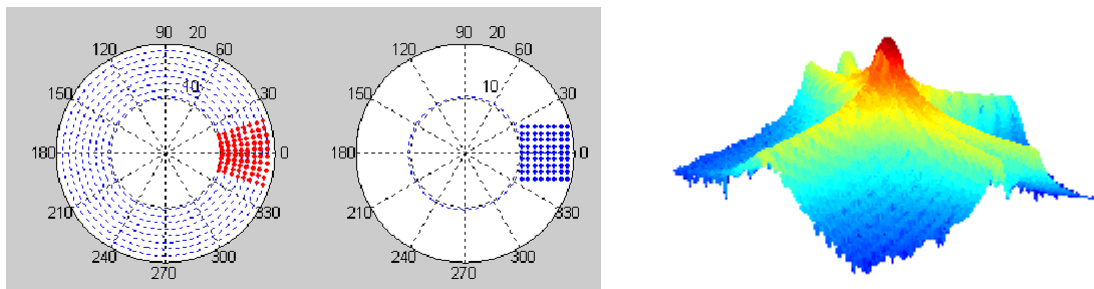


Figure 3 I Interpolation of Polar to Cartesian Space, and Imaging Impulse Response due to bandlimited data

The known effects of transforming windowed data can be applied here. For a 2D data set in $[k_x, k_y]$, the extent of k_x decides the resolution obtainable in the x-dimension of the image- here it corresponds to the down range. The applicable relation is $\delta x = 1/\Delta k_x$. Viewing along the x- axis, $\theta \approx 0, \phi \approx 0$, and $k_x = 2k$, so $\delta x = 1/2k = c/2B$ where B is the bandwidth over which data is collected.

The extent of k_y decides the resolution obtainable in the y-dimension of the image- here it corresponds to the cross-range. The applicable relation is $\delta y = 2\pi/\Delta k_y \approx 2\pi/(2k \sin \Delta\phi) \approx \lambda/(2\Delta\phi)$, where $\Delta\phi$ is the aspect angle over which data is collected.

Sampling Requirement

The finite size of the Object Space D_{span} can be used to set the sampling requirement in frequency δf and angle step size $\delta\theta$

$$\delta f = c/2D_{span}$$

$$\delta\theta = 1/2D_{span}$$

Eq 4

The step sizes used while sampling the frequency-aspect space decide the unambiguous down-range and cross-range available for creating the image.

So to be able to characterize the target's scattering over a band of frequencies, and also map its scattering spatial distribution, we need to be able to collect Far-Field RCS data over a set of aspect angles, and over a set of Frequencies, with the required sample spacing and bandwidth. Cost is very much an issue with RCS measurements- especially for large targets. A capability to make measurements in the Near Field and generate the High Resolution Images as well as Far-Field Patterns from this data would allow substantially reduced infrastructural requirements.

Near Field vs Far Field Images

In imaging, data from a small set of look-angles, and a set of frequencies is processed to generate a scattering image applicable at the central look angle and frequency. This is possible as RCS of the localized, small, individual scattering centers does not vary so much with look angle and frequency. Images reconstructed from near-field measurements are therefore almost identical to images reconstructed from far-field measurements, especially for point target (isotropic) scattering center models.

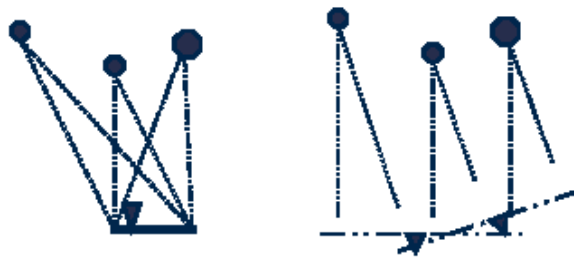


Figure 4 Angular Sectors contributing to (i) near Field Images, and (ii) Far Field Images

SAR and ISAR methods can be used to acquire multi-aspect near-field backscatter data. SAR modes can be either 'Stare' or 'Spotlight'. More generally, any kind of relative motion between target and antenna can be exploited for imaging- however the appropriate motion compensation needs to be employed.

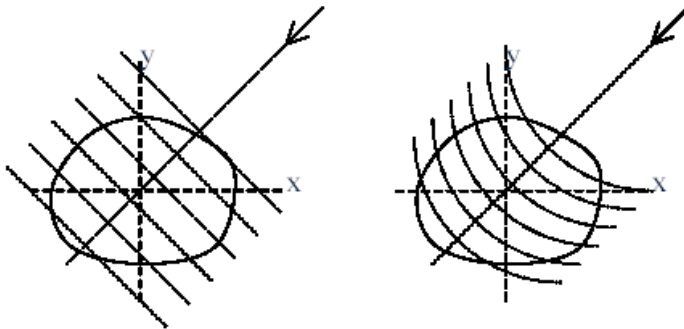


Figure 5 Far-Field (Planar) Illumination, vis-à-vis Near-Field (Spherical) Illumination

When the target is in the far-field, the illumination is planar, and image reconstruction is straightforward via Fourier Transform from polar format k -space to Object Space. When the target is in the near-field, the illumination is spherical (Figure 5), and two-way amplitude decay with range over target extent cannot be ignored. Further the amplitude variation over the target due to antenna pattern must be taken into account. So image construction is more involved and requires appropriate amplitude and phase compensation. Processing the Near Field Data to high resolution images can be carried out using the Circular Convolution technique [2], or the Tomographic method [3]. In the former, the angular domain data is processed first before integration in the frequency domain. In the second, the order is reversed. Both methods allow for amplitude compensation for range and pattern effects to be applied, and are adaptable to both SAR and ISAR imaging configurations.

For SAR imaging, the Cross-Range Resolution depends on angle subtended by the Scan length at the Object Location. It therefore degrades with increasing distance from the Scan Axis. Also, if the image is to represent the scattering map of the target as viewed along the normal to the Scan-Axis with fidelity, the scan axis must cover the extent of the target.

In conclusion, Imaging from near-field data is a valid method for the mapping of the scattering centers on a complex target. Images obtained from near-field data by and large conform to images obtained from far-field data. Limitations are observed at times when the individual scattering centers do not have RCS behaviour that is broadly invariant with look angle, as for example, extended scattering features such as edges and surfaces. However, near field imaging is associated with the very significant advantage of cost reduction. Computational overheads are insignificant with ample processing power available.

RCS from Near Field Data

Because the Near-Fields arise from the same scattering mechanisms as the far-field (the only difference being the phase factors that weight the summation elements) it is reasonable to believe that NF data should be statistically correlated to FF data. However it would be best to be able to reproduce the exact far-field RCS patterns using the Near-Field Data. How are they linked and how is this mechanism different from antenna NF to FF conversion?

By the assertions in [2], [3], and [6], the far-field RCS patterns are linked to the Near-Field Object Reflectivity Distributions via the Fourier Transform.

Polar Coordinates

$$E_{ff}(f, \vartheta) = \int_0^{\rho_{i,\max}} \int_0^{2\pi} \gamma(\rho, \varphi) e^{j4\pi(f/c)\rho \cos(\varphi - \vartheta)} d\varphi d\rho$$

Cartesian Coordinates

$$E_{ff}(f_x, f_y) = \int_{-\infty}^{\infty} \int_{-\infty}^{\infty} \gamma(x, y) e^{j2\pi(xf_x + yf_y)} dx dy$$

Eq 5

However, here we take a look at the far-field RCS pattern extraction using methods analogous to far-field antenna pattern extraction from near-field measurements. Antenna Near-Field measurement techniques have demonstrated a capability to provide far-field patterns with good accuracy from measurements made in the near-field. The Planar, Cylindrical, and Spherical Modes of near-field data collection use the corresponding modal expansions of the near-fields to compute the corresponding far-fields. It appears reasonable that antenna near-field techniques are applicable to obtain exact Far-Field RCS Patterns

In the most straightforward extension of Antenna Near Field measurements to Near-Field RCS measurements, the target is illuminated with a planar wavefront from the direction of incidence, and bistatic data collected over a planar/ cylindrical/ spherical scan surface in the near-field. These bistatic fields can then be converted to far-fields propagating in the direction of interest.

However, even if the receiving probe is in the near-field, plane-wave illumination is still required- either using a distant illuminating source antenna, or a collimating reflector, and the use of either destroys the advantage of near-field measurements in the first place. Even so there are key differences from Antenna Measurements. Antennas are highly directive, and Near-Field Measurements are typically set up so that very little energy is radiated towards the edges of the finite scan plane/ cylinder. Targets for RCS measurements are usually not designed for well-behaved scattering patterns. Antennas are excited due to the feed line, and the primary source does not directly contribute to field on the scan cylinder. In RCS measurements, background subtraction/ range gating techniques are necessary to reject the coupling of the illuminating fields into the receiver for scattered field measurements. The advantages of converting near-field scattering data to the far-field in this manner is that the method is a theoretically exact, single frequency technique. There are absolutely restrictions on the scattering model.

This method is used for cylindrical near-field RCS measurements (Figure 6), and the far-fields have been expressed in terms of the tangential fields on the scan cylinder [8].

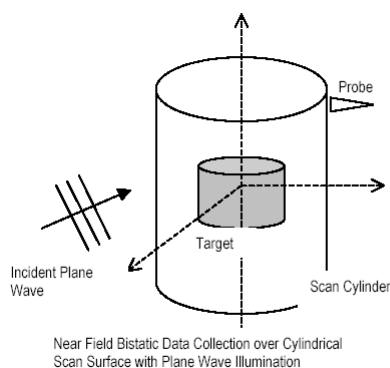


Figure 6 Schematic for Cylindrical Near-Field RCS Measurements

In a simplified representation valid for 2D target geometry infinite in the third dimension, and illuminated by a cylindrical wavefront, the object is defined in (r, ϕ) only, and the far-fields are then given by

$$E(r, \phi) = \frac{i(ka)e^{ikr}}{2\pi r} \int_0^{2\pi} \int_{-\infty}^{\infty} E_t(a, \phi') G_1(ka, \phi - \phi') d\phi' dz'$$

where

$$G_1(\alpha, \phi) = \sum_{n=-\infty}^{n=+\infty} e^{in\phi} e^{-im/2} \frac{1}{\pi\alpha H_n^{(1)}(\alpha)} \approx \cos\phi e^{i\alpha\cos\phi}, |\phi| < \frac{\pi}{2}$$

Eq 6

and the far-field RCS in this plane is

$$\sigma(\phi, k) = c_0 |E_{nf}(a, \phi) * G(ka, \phi)|^2$$

Therefore the far-fields are obtained by integrating over the scan circumference the product of the component of the near-field and the current that would be induced on a perfectly conducting cylinder that coincides with the scan cylinder and is illuminated by a plane wave that originates at the far-field observation point.

However, there is a major practical limitation of requiring planar illumination on the target. Furthermore, the Near Field probing must not disturb the target illumination. The NF probing cannot make use of target rotation, if the illumination direction is fixed. So the cost and complexity of such a near-field measurement is substantial yet. We would like to be able to both transmit and receive in the Near-Field. The implication is that a set of illumination directions in the near field will be required- to effectively synthesize a plane wave illumination. For each incident angle, the bistatic scattered data would have to be sampled over the circular aperture. It is then possible to effectively synthesize both a plane incident field and scattered field.

Using Cylindrical harmonics to expand both the incident and the scattered field, it is shown [7] that to obtain the Far-Field RCS at aspect angle θ , bistatic near field measurements are required over at least an angular sector about θ , that depends on the ratio (a/R) , where a is the max object dimension, and R is the radius at which the near-field is measured.

This appears the best that can be done with to relate far-field RCS patterns to near field RCS measurements in a rigorous manner.

An interesting treatment has been evolved [5] to work with monostatic near field data in cases when we can apply a scattering model that sums the independent contributions from the total extent of the object. Then the collected near-field data at location (ρ_0, ϕ) can be expressed as (as a function of frequency and angle)

$$E_{nf}(\phi, k) = \iint \gamma(\rho', \phi') \frac{e^{-j2kR}}{(4\pi R)^2} \rho' d\rho' d\phi'$$

$$R = \sqrt{\rho_0^2 + \rho'^2 - 2\rho_0 \rho' \cos(\phi - \phi')}$$

$$E_{ff}(\phi, k) = \iint \gamma(\rho', \phi') e^{-j2k\rho' \cos(\phi - \phi')} \rho' d\rho' d\phi'$$
Eq 7

whereas the desired far-fields correspond to summation for E_{ff} above. Then the measured near-fields are first modified by converting the two-way $(1/R^2)$ propagation factor to a one-way $(1/R)$ propagation factor, by transforming the data to the Down-Range Domain, and Range Weighting by a factor R , and back-transforming to frequency domain

$$U_{nf}(\phi, k, a) = \frac{d}{dk} E_{nf}(\phi, k) = c_1 \iint \gamma(\rho', \phi') \frac{e^{-i2kR}}{R} \rho' d\rho' d\phi'$$

$$= c_2 \int R e^{-i2kR} \left(\int E_{nf}(\phi, k') e^{i2k'R} dk' \right) dR$$
Eq 8

The modified near-fields are now in a form that allows expansion in terms of spherical wave-functions. If the Near-Fields are collected over a sphere, the same can now be converted to Far-Field RCS using spherical expansions.

Suppose the z- dimension of the target is small and the target can be modeled as effective 2D scattering distribution in the azimuth plane, and only the azimuth plane far-fields are required. It is convenient to collect near-field data only at the waterline. In [5], the near-fields have been further modified in a different way so that the source is equivalently radiating in a cylindrical (rather than spherical) manner. This is shown to amount to a Range Weighting factor of $R^{3/2}$ instead of R .

$$U(\phi, k) = c_3 \int R^2 H_0^{(1)}(2kR) \left(\int E_{nf}(\phi, k') e^{-i2k'R} dk' dR \right)$$

$$= c_3 \int R^2 \sqrt{\frac{1}{i\pi kR}} e^{i2kR} \left(\int E_{nf}(\phi, k') e^{-i2k'R} dk' dR \right)$$

$$= c_4 \int R^{3/2} \left(\int E_{nf}(\phi, k') e^{-i2k'R} dk' dR \right) e^{i2kR}$$
Eq 9

Now the modified data can be propagated to far-field in a manner similar to cylindrical modes in antenna near-fields. The far-fields can be computed by convolving the modified near-fields, as in Eq 6 with functions describing the current that would be induced on a perfectly conducting cylinder that coincides with the scan cylinder and is illuminated by a plane wave that originates at the far-field observation point

Here, unlike for the rigorous methods, multifrequency data is essentially required to compute the Far-Field RCS at even one frequency. This is not necessarily a problem, because multi-frequency is anyway acquired for generating High Resolution Images of the Target, and applying Range Gates. Range Gating is inevitably used during RCS measurements to remove clutter from outside the Range of Interest. Also the availability of multi-frequency data helps in extracting RCS statistics – histograms, percentile levels etc

Simulations on point scatterer models show very good agreement between the NF to FF converted data and the simulated FF data. Figure 7 (i) shows simulations for a Point Target offset from Center of Rotation by 2m, $R_0=5$ m,

$f_0=3$ GHz. The FF pattern does not change with any offset in target position. Figure 7(ii) shows simulations on an Extended Target of 2 m length, offset from the Center of Rotation by 40 cm, $R_0=5$ m, $f_0=6$ GHz

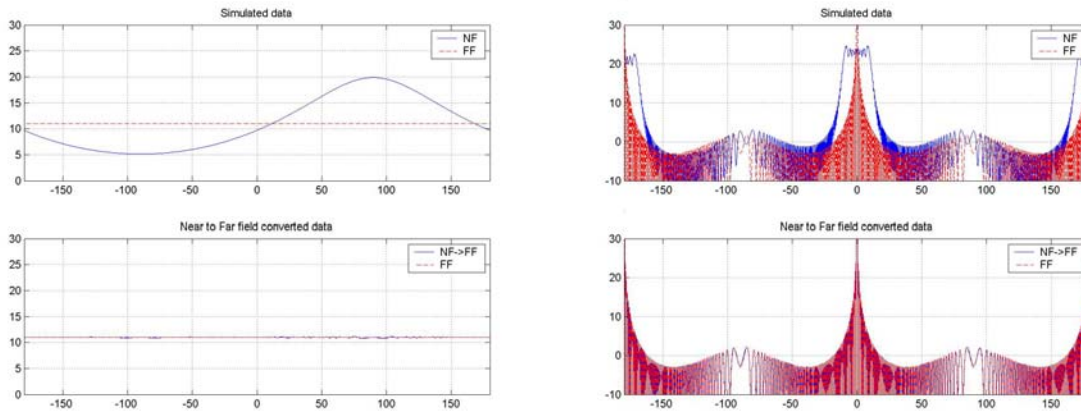


Figure 7 Simulated Monostatic NF (blue) to FF (red) conversion for (i) point target, (ii) cylindrical target

The sidelobe structure is nicely reproduced, as seen in a zoomed view in Figure 8(i).

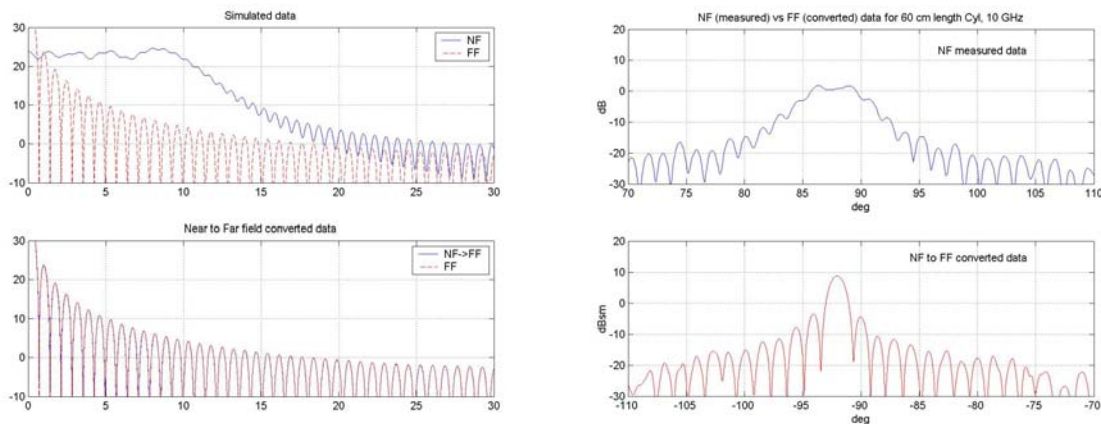


Figure 8 (i) Zoomed view on NF to FF conversion of simulated cylinder data (ii) Application to measured data

Figure 8 (ii) shows actual measurements on a 60 cm long cylinder, with 30 cm dia, at X-Band Conversion of NF data to Far-Field pattern is along expected lines. Deviations from the ideal pattern are a result of the quality of measured NF data.

This technique has assumed independent scattering from the various contributors to the composite RCS. Also the actual reflectivity mapping is modified by means of a range-weighting before the equivalent near-to-far field conversion takes place. Scattering mechanisms that do not satisfy the above model will be incorrectly transformed. Notably cavity scattering mechanisms give rise to extended range artifacts which ought not to be range weighted in the manner above. Another point to note is that in this 2D version, the vertical extent of the target has been assumed to be small and so it is actually the projected reflectivities on the horizontal plane that are contributing to the far-field. That said, very reasonable correspondence is observed for Far-Fields as computed from measured/ simulated Near Field data for known targets.

All the other factors affecting measurement errors are common to both near- and far field measurements. However near-field methods have a decided advantage over far-field measurements- which are more complex- either requiring a very large range and high transmit power, or large collimators. Near-Field measurements are very cost effective for large object RCS measurements.

The Near Field methods outlined here have been explored in an attempt to implement low-cost methods for RCS studies on large targets- much of it at DRDO's Near Field Diagnostic RCS Facility (NFDRF) at Jodhpur- a measurement facility for aircraft as well as a Testbed for developing measurement methods and techniques. The NFDRF Facility is equipped to acquire monostatic backscatter data in both SAR and ISAR configurations. The Range provides Near-Field 2D Images for diagnostic studies and estimates of Far-fields using statistical methods and the monostatic NF-to-FF conversion methods.

References

1. "Evaluation of Bistatic Far-Field Quantities from Near-Field Measurements", JL Leou, HJ Li, PIER 25, 2000
2. "Spherical wave near-field imaging and radar cross-section measurement", A Broquetas et al, IEEE Trans AP-46, May 1998.
3. "Radar Cross-Section Measurements using Near-Field Radar Imaging", JW Odendaal, J Joubert, IEEE Trans AP-45, Dec 1996.
4. "Antenna Pattern Compensation for Near Field to Far Field RCS Transformation of 1D Linear SAR Measurements", AMTA 2003
5. "Improved Version of the Circular Near-Field to Far-Field Transformation (CNFFFT)", La Haie et al, AMTA 2005
6. "Comparison and Application of Near-Field ISAR Imaging Techniques for Far-Field Radar Cross Section Determination", T Vaupel, T Eibert, IEEE Trans AP, Jan 2006
7. "Effective Estimation of 2D Monostatic Radar Cross-Section from Near-Field Measurements", IEEE Trans AP, Feb 2006
8. "Bistatic RCS Calculations from Cylindrical Near-Field Measurements- Part 1: Theory", TB Hansen et al. IEEE Transactions Antennas & Propagation, Vol 54, December 2006